Nanocrystalline Precursors for the Co-Assembly of Crack-Free Metal Oxide Inverse Opals

*Katherine R. Phillips, Tanya Shirman, Elijah Shirman, Anna V. Shneidman, Theresa M. Kay, and Joanna Aizenberg**

Inorganic microstructured materials are ubiquitous in nature. However, their formation in artificial self-assembly systems is challenging as it involves a complex interplay of competing forces during and after assembly. For example, colloidal assembly requires fine-tuning of factors such as the size and surface charge of the particles and electrolyte strength of the solvent to enable successful self-assembly and minimize crack formation. Co-assembly of templating colloidal particles together with a sol–gel matrix precursor material helps to release stresses that accumulate during drying and solidification, as previously shown for the formation of high-quality inverse opal (IO) films out of amorphous silica. Expanding this methodology to crystalline materials would result in microscale architectures with enhanced photonic, electronic, and catalytic properties. This work describes tailoring the crystallinity of metal oxide precursors that enable the formation of highly ordered, large-area (mm^2) crack-free titania, zirconia, and alumina IO films. The same bioinspired approach can be applied to other crystalline materials as well as structures beyond IOs.

Nature creates complex microstructures with advanced functionality by controlling the chemistry and morphology of the nanoscale building blocks. In order to achieve high-quality microscale architectures using synthetic self-assembly, the material precursors must also be carefully tailored. One of the most popular natural and synthetic self-assembled materials, opals, are periodic porous structures created through assembly of monodisperse spherical sub-micrometer colloidal particles, which are often used as a template to form inverse opals (IOs). These structures exhibit unique optical, mechanical, and fluidic properties,[1] but a high degree of control over their composition and quality is important for many of their applications, including nonfading pigments,[2] color displays,[3] solar cells,[4] catalysts,[1e,5] and filtration membranes.[6] Structural defects, such as cracks, can be detrimental to IO's performance in these applications, as they lead to optical scattering and fluid escape paths. In order to avoid such defects, nature often utilizes soft, typically organic, entities to direct the deposition of inorganic materials.[7] Inspired by this strategy, our group previously introduced a co-assembly method, in which templating colloidal particles and matrix precursor materials are deposited simultaneously from a single assembly mixture to produce defect-free IO films over centimeter scales.[8] Co-assembly mitigates crack formation during the drying process due to the presence of mobile colloidal particles (Figure S1, Supporting Information), in contrast to the rigid template for the typical alternative approach, which involves backfilling a pre-formed colloidal template, and which results in high-quality domains of no more than 10–100 μm in each direction.[9]

Co-assembly has enabled crack-free IOs out of amorphous materials such as silica. By extending the co-assembly process to crystalline metal oxides, such as titania and alumina, the benefits of long-range order can be combined with inherent materials properties, that is, high refractive index and catalytic activity. Additionally, fundamental questions related to photonic-enhanced photocatalysis[10] and band-edge lasing[11] could be investigated with defect-free IO films. However, the formation of such metal oxide IOs remains a challenge in part due to the amorphous-to-crystalline phase transition and associated crystallization-induced volume shrinkage of solid matrix during the heat treatment, whether purely crystalline precursors,[12] amorphous sol–gel precursors,[13] or a combination of both[14] are used. Metal oxide sol–gel precursors present the additional challenge of high hydrolytic instability.[15]

Nature again provides inspiration as we look to expand the scope of IO composition to include crystalline materials. One of the central biomineralization principles is to pre-assemble nanoscale building blocks with controlled surface charge, size, shape, and crystallinity.[7] In particular, the formation of crystalline and amorphous phases that coexist in mineralized tissues is a common, very general biomineralization principle that endows crystalline biomaterials with high order and mechanical stability.[16] By combining amorphous ("soft")

Dr. K. R. Phillips, Prof. J. Aizenberg
Department of Chemistry and Chemical Biology
Harvard University
Cambridge, MA 02138, USA
E-mail: jaiz@seas.harvard.edu
Dr. T. Shirman, Dr. E. Shirman, Dr. A. V. Shneidman, T. M. Kay, Prof. J. Aizenberg
John A. Paulson School of Engineering and Applied Sciences
Harvard University
Cambridge, MA 02138, USA
Dr. T. Shirman, Dr. E. Shirman, Prof. J. Aizenberg
Wyss Institute for Biologically Inspired Engineering
Harvard University
Cambridge, MA 02138, USA
The ORCID identification number(s) for the author(s) of this article can be found under https://doi.org/10.1002/adma.201706329.

DOI: 10.1002/adma.201706329

and crystalline ("hard") components with optimized ratio and dimensions of the building blocks, nature forms structures with fine features that experience minimal structural changes during densification and phase transitions.[17]

This work describes a generalized approach for the co-assembly of crack-free metal oxide (titania, zirconia, and alumina) IO films using precursors designed with the same biomineralization principle (**Figure 1**). We report that a careful choice of nanocrystalline metal oxide precursors (NCs) containing finely controlled proportions of crystalline and amorphous phases allows this goal to be achieved. As discussed in the Supporting Information and shown in Figures S1–S3 (Supporting Information), the amorphous portion of the NCs mitigates stresses arising during the colloidal assembly process, and the crystalline component minimizes large volume shrinkage arising during calcination-induced phase transitions. Furthermore, we demonstrate the applicability of this method to grow inverse opal films on flexible substrates as well as to incorporate additional functional nanoparticles.

We begin our demonstration with the detailed discussion of the formation of uniform, crack-free titania IOs. A published peptization process[18] provided control over titania NC size, morphology, and their amorphous fraction. The synthesis procedure is based on hydrolysis and polycondensation of titanium alkoxide in the presence of tetramethylammonium hydroxide (TMAH).[18] It has been suggested that TMAH catalyzes a complete hydrolysis of alkoxide groups and provides an organic cation to assist and direct the polycondensation process (nucleation and growth), by stabilizing the intermediate structural units or clusters (see the Supporting Information for more details).[18] Here, a constant amount (41.3×10^{-3} M) of titanium isopropoxide (TIP) in 2-propanol was added dropwise to a precooled aqueous solution of TMAH; the concentration of TMAH was varied to achieve molar ratios of TIP to TMAH ($R_{TIP/TMAH}$) between 0.3 and 2.0. The reaction mixture was then refluxed, cooled, and allowed to age for specific times. The resulting suspended precursors were dried and subsequently characterized by transmission electron microscopy (TEM), Raman spectroscopy, X-ray diffraction (XRD), X-ray photoelectron spectroscopy (XPS), thermal gravimetric analysis (TGA), and differential scanning calorimetry (DSC). Both the concentration of TMAH and the aging of the particles were shown to affect the NC size and morphology.

TEM and Raman spectra indicate that titania is present in the anatase phase. TEM images show crystalline particles for all $R_{TIP/TMAH} > 0.3$; however, both the degree of crystallinity and the NC size depend on TIP/TMAH molar ratio and aging (Figure S4, Supporting Information). As shown in **Figure 2**A–C, the lattice planes have an interplanar distance of 3.5 Å for $R_{TIP/TMAH} = 1$ and 1.4, corresponding to the (101) planes of the anatase crystal structure.[19] Raman spectroscopy further confirms the presence of the anatase phase (Figure 2D), with the primary characteristic anatase E_g Raman modes visible at ≈146 cm^{-1} for $R_{TIP/TMAH} > 1.4$. NCs with $R_{TIP/TMAH} = 0.5$ and 1.0 show no anatase Raman peaks despite the TEM results, which we attribute to the presence of a large amount of amorphous titania. In terms of morphology, NCs with $R \leq 1.4$ ratio are ≈5 nm in size, with nearly spherical shape. For higher TIP/TMAH ratios, the NCs increase in size (to ≈20–30 nm for $R_{TIP/TMAH} = 2$) and form elongated fibers (Figure S5, Supporting Information). The increase of the crystallite size is further confirmed by the shift in the main E_g Raman band frequency, as shown in the inset of Figure 2D, in accordance with the phonon confinement model.[20] Aging time also influences the crystallinity and morphology of the titania NCs, as discussed in more detail in the Supporting Information.

In order to gain insight into the relative amounts of amorphous and crystalline components of the titania NCs, we performed XPS, TGA, and DSC to probe the degree of condensation of $Ti(OH)_x$ species in different NCs. XPS measurements were performed on dried NCs of different TIP/TMAH ratios after one month of aging. All studied samples exhibited O:Ti ratio between ≈2.2 and ≈3.5 (well over the stoichiometric value of 2.0 for TiO_2), which decreased noticeably for higher TIP/TMAH ratios (Figure 2E). Dried samples were also analyzed with TGA and DSC up to 1400 °C (Figure S6, Supporting Information). The weight loss at ≈500 °C in the TGA spectra corresponds to polycondensation and crystallization of hydrated titania into the anatase phase, which can be assigned to the first broad exothermic peak on the DSC curve. Comparing the TGA/DSC data, a clear trend can be observed: the final weight loss decreases for higher TIP/TMAH ratios (lower TMAH concentrations). A quantitative comparison of the amorphous fraction, *F*, for samples aged for one month, was estimated according to Equation (1) and plotted in Figure 2F:

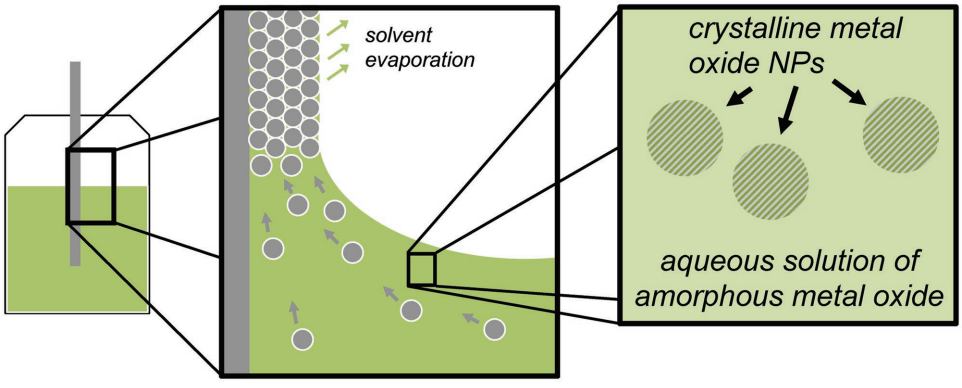

Figure 1. Schematic of co-assembly process via evaporation-induced deposition of templating colloids and metal oxide (e.g. titania) precursor on a vertical substrate. The nanocrystalline precursor consists of a metal oxide comprising various crystalline and amorphous phases.

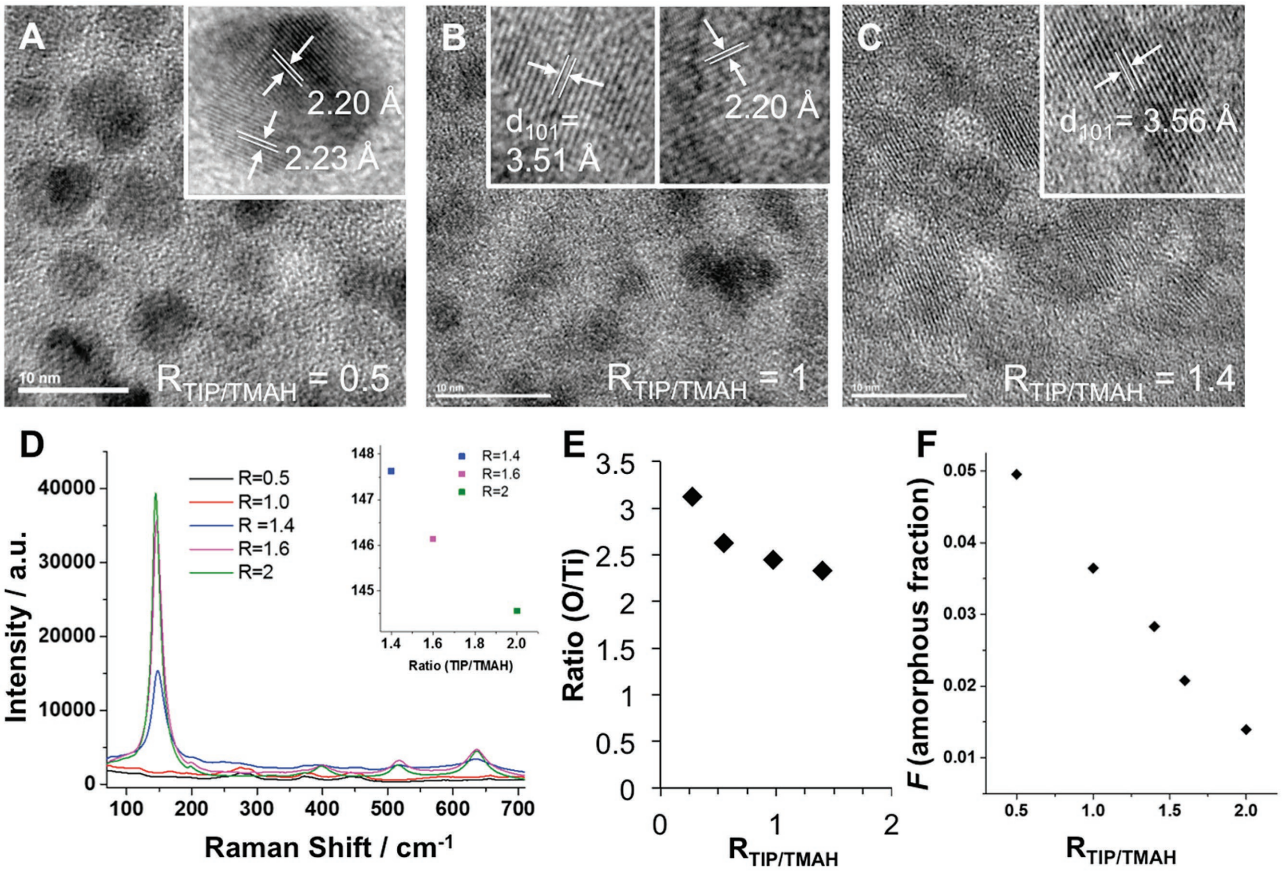

Figure 2. Imaging and characterization of as-synthesized titania nanocrystalline precursors made with different ratios ($R_{TIP/TMAH}$) of titanium precursor (titanium isopropoxide, TIP) to base (tetramethylammonium hydroxide, TMAH). TEM images of nanocrystals with $R_{TIP/TMAH}$ of: A) 0.5, B) 1, and C) 1.4, all after 7 d aging. Analytical spectroscopy: D) Raman spectra of titania nanocrystalline precursors prepared using various $R_{TIP/TMAH}$ before calcination, with aging time of 7 d; inset shows red-shift (to lower cm^{-1}) of the characteristic anatase titania peak frequencies with increasing $R_{TIP/TMAH}$. E) Ratio of O to Ti, as determined by X-ray photoelectron spectroscopy (XPS) for different $R_{TIP/TMAH}$. F) The amorphous fraction, *F*, obtained from thermal gravimetric analysis.

$$F = \frac{(\text{weight at } 200\ ^\circ\text{C}) - (\text{weight at } 1000\ ^\circ\text{C})}{(\text{weight at } 1000\ ^\circ\text{C})} \quad (1)$$

These results support our hypothesis that higher TIP/TMAH ratios have more titania in the form of anatase crystallites. In addition to TGA and DSC, temperature effects were probed by analyzing the NCs after calcination at 500 °C with Raman and XRD (Figures S6 and S7, Supporting Information). The spectral peaks indicate that only the anatase phase of titania is formed in this temperature range. The second exothermic peak on the DSC curve, at ≈1200 °C, was attributed to the phase transformation from anatase to rutile (see the Supporting Information for more discussion).

The quality of the titania IOs co-assembled using the as-prepared NC suspension is a function of the NC properties. Depending on the titania NCs' $R_{TIP/TMAH}$ and aging, crack-free titania IO films can form (**Figure 3**). For the lowest TIP/TMAH ratios investigated, both the excess of TMAH and lack of crystalline phase result in the crack formation ($R_{TIP/TMAH}$ = 0.3, Figure S8, Supporting Information). High concentrations of charged molecules such as TMAH can interfere with intercolloidal particle repulsive forces, causing the formation of disordered films or aggregated solutions, such as those seen for $R_{TIP/TMAH}$ = 0.3. For NCs with $R_{TIP/TMAH}$ = 0.5 and above, the lower amount of TMAH produces ordered and crack-free IO films before calcination (Figure S9, Supporting Information); however, the short (1 d) NC aging times with the TIP/TMAH ratio of 0.5 yielded cracked IO films, which we attribute to an insufficient amount of crystalline titania. Aging for 7 d significantly improves the quality of the film, leading to crack-free IO films (Figure 3A).

Higher ratios ($R_{TIP/TMAH}$ = 1, 1.4, 1.6) give rise to the formation of crack-free IO films for aging times above one month. The low concentration of TMAH does not disrupt the assembly, the presence of amorphous titania helps to accommodate stress during drying, and a sufficient amount of crystalline phase prevents volume shrinkage during the calcination. For NC synthesized from high TIP/TMAH ratios (such as $R_{TIP/TMAH}$ = 2), an increase in crack formation of the resulting IO films was observed for longer aging times. Only a freshly prepared precursor gives rise to the crack-free IO, whereas aging times longer than 1 d produce films exhibiting cracks for these high-*R* precursors. The cracks are formed during the

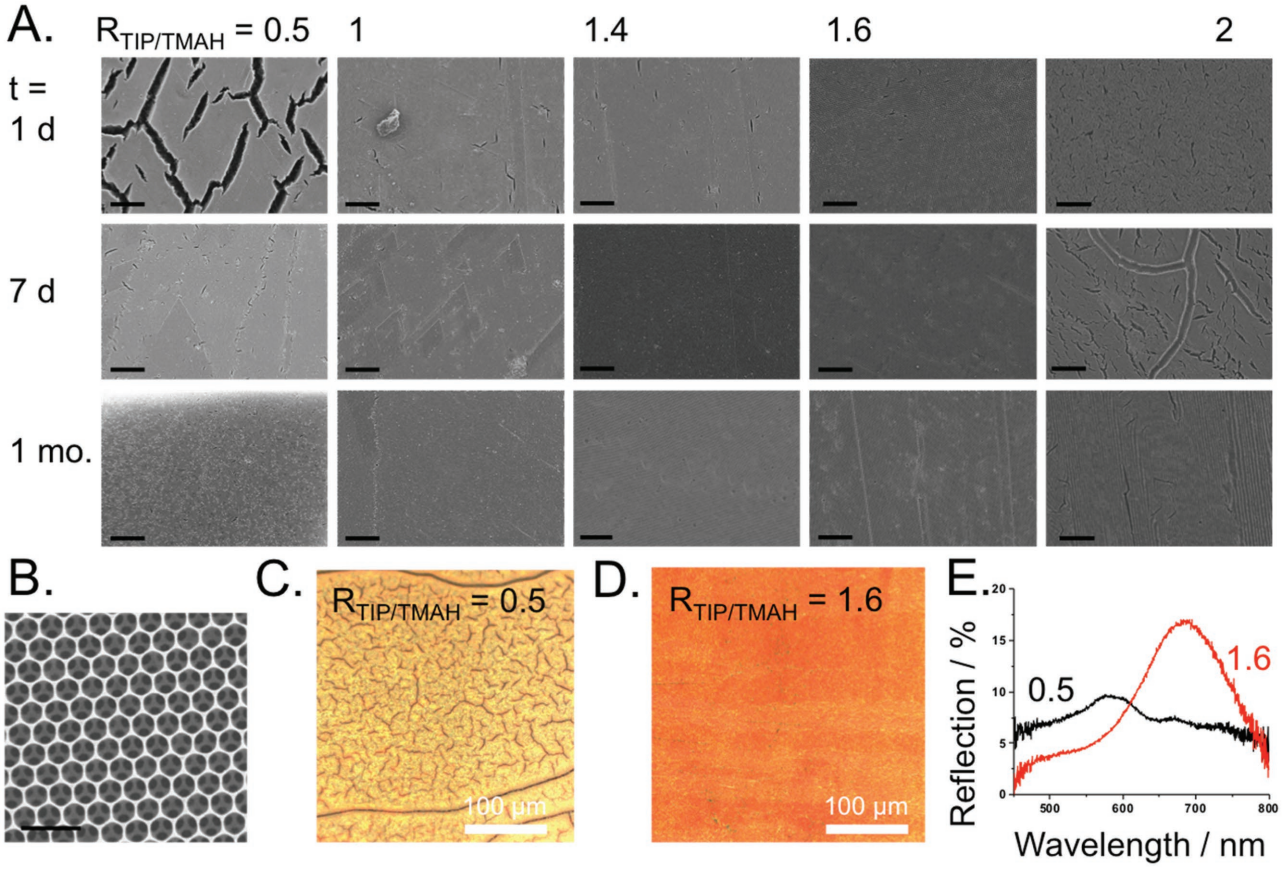

Figure 3. Inverse opal films made from various titania nanocrystals. A) SEM images of titania inverse opal films, where each column corresponds to a different $R_{TIP/TMAH}$ ratio. Each row represents a different aging time. Scale bars are 10 µm. B) SEM image of titania inverse opal film synthesized using NCs with $R_{TIP/TMAH}$ = 0.5 and 7 d aging. Scale bar is 1 µm. C,D) Optical images, and E) corresponding optical spectra, of titania inverse opal films made from NCs synthesized with ratios ($R_{TIP/TMAH}$) of 0.5 (C) and 1.6 (D), and 1 mo. aging time; scale bars are 100 µm. All samples underwent calcination at 500 °C.

co-assembly process (Figure S9D, Supporting Information), which we attribute to the large size of the titania NC precursors. From this analysis, we conclude that an amorphous fraction, *F*, between 0.02 and 0.05 is necessary to co-assemble crack-free titania IO films. All films exhibit high order (Figure 3B). To examine the effect of high temperature on the structural integrity, titania inverse opal films (synthesized from NC's with $R_{TIP/TMAH}$ = 1, 14 d aging) were calcined at 700 °C. The resulting films retain their spherical pore structure and showed no cracking (Figure S10, Supporting Information).

Optical characterization of IOs fabricated using different NCs reveals the formation of either visible cracks (Figure 3C) or high-quality crack-free films (Figure 3D) for representative precursors made with $R_{TIP/TMAH}$ of 0.5 and 1.6, respectively, both with one month aging time. The quality of the film also affects the reflection spectra (Figure 3E). The cracks in the sample made from the lower $R_{TIP/TMAH}$ show low-intensity reflection peaks compared to samples made from higher $R_{TIP/TMAH}$, in addition to less vibrant colors visible in the optical images, as expected based on the cracking seen in SEM. For titania NCs made with $R_{TIP/TMAH}$ = 1.8, a characteristic refractive index of the anatase phase of 2.23 was measured using ellipsometry (Figure S11, Supporting Information). As expected, in contrast to silica IO,[8b] titania IOs retain color in liquids upon infiltration (Figure S12, Supporting Information) due to the high refractive index of titania, which does not match that of the liquid.

This process of fabricating crack-free metal oxide inverse opal films can be applied to manufacturing various functional materials with highly desired properties and promising applications. For example, formation of titania IOs is particularly relevant for catalysis and electrode applications.[1c,e,5b] Using co-assembly, we can also incorporate functional nanoparticles into the IO matrix.[2b,21] For example, by adding negatively charged (citrate-capped) gold nanoparticles (AuNP) to the NC titania precursor, we fabricated highly ordered hybrid inverse opal films with homogeneously distributed AuNP (Figure 4A,B). Hybrid metal oxide support/metal nanoparticle systems are used extensively in catalysis,[5b] and titania-AuNP IOs are particularly promising photocatalytic systems.[9a]

Furthermore, titania IO films may also find applications in the field of electrochromic (EC) devices, due to significantly faster switching times and enhanced coloration contrasts.[22] Such films are conventionally made by atomic layer deposition (ALD) on transparent substrates, for example, indium tin oxide (ITO)-coated glass. However, the substrate choice is limited by the high temperatures that are typically required to crystallize

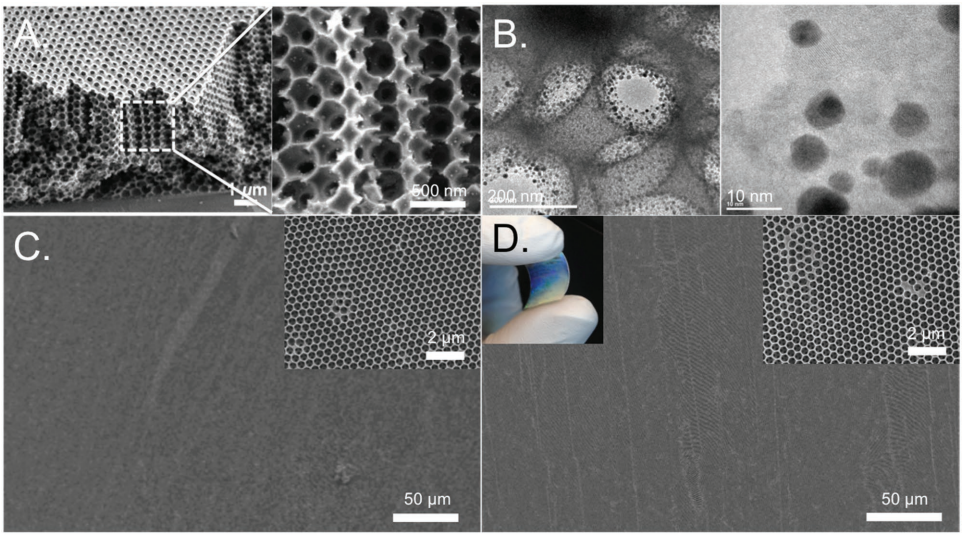

Figure 4. A,B) SEM (A) and TEM (B) of a titania IO film with incorporated gold nanoparticles. C,D) SEM images of a large-area, crack-free titania IO film on a conductive plastic substrate (ITO/PET), before bending (C), and after bending (D). Right insets show higher magnification SEM images. Left inset in (D) is a photograph of the bending.

the matrix material and remove the templating colloids, preventing the use of inexpensive, lightweight, and flexible substrates.[23] The crystalline character of our NC precursors allows us to avoid the calcination step, instead removing the colloids by dissolution in organic solvent such as toluene. As a demonstration, we fabricated large-area crack-free titania inverse opal films on ITO-coated flexible poly(ethylene terephthalate) (ITO/PET) substrates (**Figure 4**C,D) that would otherwise degrade at high temperatures. As shown in the left inset of Figure 4D, titania inverse opal films on ITO/PET substrates retain their integrity while bent, and SEM imaging confirms that the inverse opal structure remains intact after bending (Figure 4D).

The TMAH-based peptization process described here can be directly extended to metal oxides beyond titania, and we demonstrate such synthesis for two other practically important materials, zirconia and alumina. Zirconium isopropoxide and aluminum isopropoxide were substituted for titanium isopropoxide in the NC synthesis procedure to make zirconia and alumina NCs, respectively (**Figure 5**). TEM images reveal that the resulting nanoparticles are crystalline and several nanometers

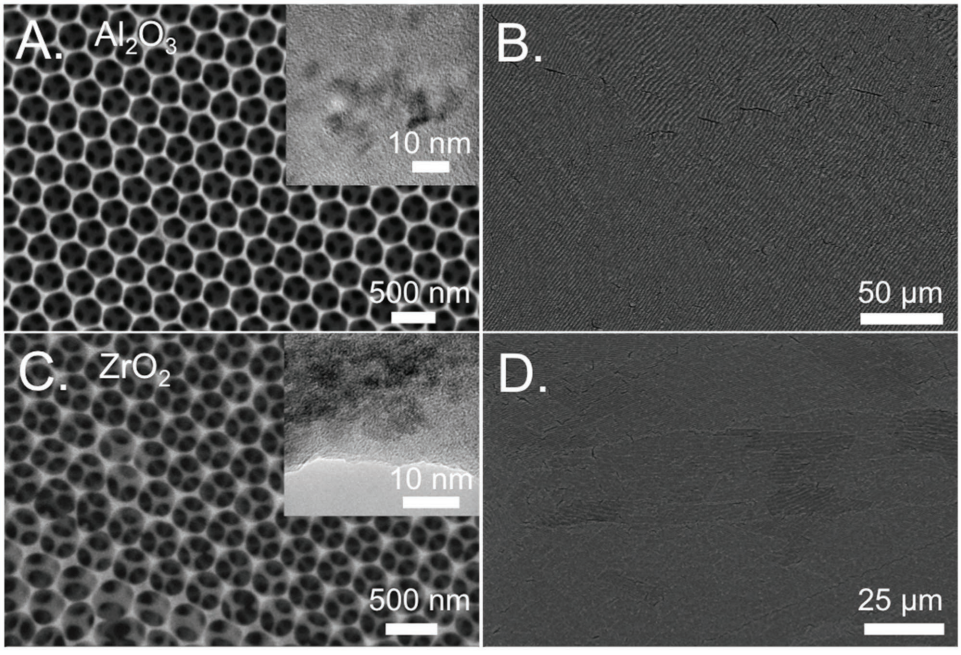

Figure 5. A–D) Representative images of inverse opal films made from alumina (A,B) and zirconia (C,D), grown on silicon substrates using (A, inset) Al_2O_3 nanocrystals and (C, inset) ZrO_2 nanocrystals, respectively. Large images are SEMs, insets are TEMs.

in diameter (Figure 5A,C, insets). The SEM images show the crack-free quality of the thus-assembled IO films (Figure 5). The composition of the inverse opal films was confirmed using EDS and XRD (Figures S13 and S14, Supporting Information).

In summary, crack-free titania, alumina, and zirconia IOs were co-assembled using carefully designed NC precursors. Building on biomineralization principles, where the combination of nanocrystalline and amorphous mineral phases give rise to oriented, high-quality crystals,[16] we design our precursors to contain a mixture of nanocrystalline and amorphous metal oxide phases. Having both components allows the precursor to accommodate stresses during the self-assembly process and to minimize volume changes during phase transitions, leading to high-quality inverse opal films: the crystalline phase suppresses crack formation during calcination, and the hydrated amorphous phase suppresses crack formation during the drying stage. It is noteworthy that neither the assembly of purely crystalline precursor phase[12] nor the use of sol–gel amorphous precursors[13] nor a simple combination of both[14] allows for the formation of such ordered, defect-free crystalline metal oxide films. These crack-free IOs enable or enhance a range of applications, such as photocatalysis[10] and band-edge lasing.[11] We furthermore extended the fabrication procedure to IO films formed on flexible substrates and with additional functional particles (e.g., catalytic nanoparticles). Such crack-free films can be used in model studies in which the effect of the structure can be isolated and decoupled from the interference from defects. We believe that the presented methodology for the formation of NC/amorphous precursors can be broadly applied to other crystalline materials, and to the fabrication of a variety of nanoscale structures.

Experimental Section

Nanocrystal Synthesis: Titania NCs were synthesized by modifying a peptization synthesis procedure from the literature.[18] For each batch, 25% tetramethyl ammonium hydroxide (TMAH; up to 4.6 mL) was added to water (90 mL) in an ice bath. The exact volume of TMAH was adjusted as described in the text to achieve a desired molar ratio of TIP to TMAH ($R_{TIP/TMAH}$). TIP (1.1 mL) in isopropanol (15 mL) was added dropwise to the cooled TMAH solution under stirring. After ≈10 min, the flask containing the reaction mixture was submerged in a silicone oil bath heated above 100 °C, and the solution was left under reflux with a condenser for 6 h. During this time, a white gel-like precipitate formed, which slowly dissolved upon reflux. After reflux, the NCs were cooled to room temperature and the resulting suspension was used without further purification, either immediately or after aging for various lengths of time. The same procedure was followed for alumina and zirconia precursors by substituting aluminum isopropoxide and zirconium isopropoxide, respectively, for TIP using the same molar ratios.

Inverse Opal Assembly: IOs were made using a modified co-assembly procedure described previously.[8a] Briefly, the assembly solution consisted of acrylic-acid-capped polystyrene (PS) spheres, prepared following a literature procedure,[24] that were diluted to 0.1 wt% and mixed with the as-synthesized titania, alumina, or zirconia NCs (40 µL per mL of the assembly solution. When used, 100 µL of citrate-capped AuNP were added per mL of the assembly solution. A silicon wafer or glass slide was used as substrate, which underwent plasma cleaning prior to use. For the samples grown on ITO/PET, the ITO-coated plastic substrates were first cleaned for 3 min in an ultrasonic bath in acetone, ethanol, and deionized water, successively, then dried, and finally plasma-treated for 1 min. The substrate was vertically submerged into the assembly solution in a vial and placed in a 65 °C oven undisturbed for two days for the co-assembly process to occur. Typically, the samples next underwent calcination at 500 °C for 2 h to sinter the matrix and remove the PS template. For samples grown on ITO/PET, the PS colloids were removed by dissolution in toluene.

Supporting Information

Supporting Information is available from the Wiley Online Library or from the author.

Acknowledgements

K.R.P. and T.S. contributed equally to this work. The authors acknowledge Dr. Alison Grinthal and Dr. Michael Aizenberg for thoughtful discussions and assistance with the manuscript. K.R.P. acknowledges support from a graduate fellowship from the Department of Defense. T.S. acknowledges support from the Weizmann Institute of Science—National Postdoctoral Award Program for Advancing Women in Science. The materials design aspects of this work are supported by the National Science Foundation (NSF) Designing Materials to Revolutionize and Engineer our Future program under Award No. DMR 1533985. Electron microscopy and other characterizations were performed in part at the Harvard University Center for Nanoscale Systems (CNS), a member of the National Nanotechnology Coordinated Infrastructure Network (NNCI), which is supported by the National Science Foundation under NSF ECCS Award No. 1541959.

Conflict of Interest

The authors declare no conflict of interest.

Keywords

inverse opals, metal oxide nanocrystals, self-assembly

Received: October 31, 2017
Revised: November 29, 2017
Published online:

[1] a) J. F. Galisteo-Lopez, M. Ibisate, R. Sapienza, L. S. Froufe-Perez, A. Blanco, C. Lopez, *Adv. Mater.* **2011**, *23*, 30; b) N. D. Petkovich, A. Stein, *Chem. Soc. Rev.* **2013**, *42*, 3721; c) K. R. Phillips, G. T. England, S. Sunny, E. Shirman, T. Shirman, N. Vogel, J. Aizenberg, *Chem. Soc. Rev.* **2016**, *45*, 281; d) A. Stein, F. Li, N. R. Denny, *Chem. Mater.* **2008**, *20*, 649; e) A. Stein, B. E. Wilson, S. G. Rudisill, *Chem. Soc. Rev.* **2013**, *42*, 2763; f) G. von Freymann, V. Kitaev, B. V. Lotsch, G. A. Ozin, *Chem. Soc. Rev.* **2013**, *42*, 2528.

[2] a) D. P. Josephson, M. Miller, A. Stein, *Z. Anorg. Allg. Chem.* **2014**, *640*, 655; b) N. Koay, I. B. Burgess, T. M. Kay, B. A. Nerger, M. Miles-Rossouw, T. Shirman, T. L. Vu, G. England, K. R. Phillips, S. Utech, N. Vogel, M. Kolle, J. Aizenberg, *Opt. Express* **2014**, *22*, 27750.

[3] a) T. Ito, C. Katsura, H. Sugimoto, E. Nakanishi, K. Inomata, *Langmuir* **2013**, *29*, 13951; b) S. Y. Lee, S. H. Kim, H. Hwang, J. Y. Sim, S. M. Yang, *Adv. Mater.* **2014**, *26*, 2391.

[4] a) X. Chen, J. Ye, S. Ouyang, T. Kako, Z. Li, Z. Zou, *ACS Nano* **2011**, *5*, 4310; b) S. Guldin, S. Huttner, M. Kolle, M. E. Welland,

P. Muller-Buschbaum, R. H. Friend, U. Steiner, N. Tetreault, *Nano Lett.* **2010**, *10*, 2303; c) J. W. Lee, J. Lee, C. Kim, C. Y. Cho, J. H. Moon, *Sci. Rep.* **2014**, *4*, 6804; d) J. W. Lee, J. H. Moon, *Nanoscale* **2015**, *7*, 5164.

[5] a) C. M. Parlett, M. A. Isaacs, S. K. Beaumont, L. M. Bingham, N. S. Hondow, K. Wilson, A. F. Lee, *Nat. Mater.* **2016**, *15*, 178; b) E. Shirman, T. Shirman, A. V. Shneidman, A. Grinthal, K. R. Phillips, H. Whelan, E. Bulger, M. Abramovitch, J. Patil, R. Nevarez, J. Aizenberg, *Adv. Funct. Mater.* **2017**, https://doi.org/10.1002/adfm.201704559; c) Y. Wang, H. Arandiyan, J. Scott, M. Akia, H. Dai, J. Deng, K.-F. Aguey-Zinsou, R. Amal, *ACS Catal.* **2016**, *6*, 6935.

[6] a) D. Li, J. Yao, H. Wang, *Thin Films and Membranes with Hierarchical Porosity*. In: *Encyclopedia of Membrane Science and Technology*, Wiley, New York **2013**; b) X. Wang, S. M. Husson, X. Qian, S. R. Wickramasinghe, *J. Membr. Sci.* **2010**, *365*, 302; c) S. J. Yeo, G. H. Choi, P. J. Yoo, *J. Mater. Chem. A* **2017**, *5*, 17111.

[7] a) L. Addadi, S. Weiner, *Angew. Chem., Int. Ed. Engl.* **1992**, *31*, 153; b) P. U. P. A. Gilbert, M. Abrecht, B. H. Frazer, *Rev. Mineral. Geochem.* **2005**, *59*, 157; c) C. Rodriguez-Navarro, E. Ruiz-Agudo, J. Harris, S. E. Wolf, *J. Struct. Biol.* **2016**, *196*, 260; d) S. Weiner, L. Addadi, *Annu. Rev. Mater. Res.* **2011**, *41*, 21.

[8] a) B. Hatton, L. Mishchenko, S. Davis, K. H. Sandhage, J. Aizenberg, *Proc. Natl. Acad. Sci. USA* **2010**, *107*, 10354; b) I. B. Burgess, N. Koay, K. P. Raymond, M. Kolle, M. Loncar, J. Aizenberg, *ACS Nano* **2012**, *6*, 1427.

[9] a) Z. Cai, Z. Xiong, X. Lu, J. Teng, *J. Mater. Chem. A* **2014**, *2*, 545; b) J. I. L. Chen, G. von Freymann, S. Y. Choi, V. Kitaev, G. A. Ozin, *Adv. Mater.* **2006**, *18*, 1915; c) K. Kim, P. Thiyagarajan, H. J. Ahn, S. I. Kim, J. H. Jang, *Nanoscale* **2013**, *5*, 6254; d) J. Liu, M. Li, J. Wang, Y. Song, L. Jiang, T. Murakami, A. Fujishima, *Environ. Sci. Technol.* **2009**, *43*, 9425.

[10] M. Curti, J. Schneider, D. W. Bahnemann, C. B. Mendive, *J. Phys. Chem. Lett.* **2015**, *6*, 3903.

[11] a) J. P. Dowling, M. Scalora, M. J. Bloemer, C. M. Bowden, *J. Appl. Phys.* **1994**, *75*, 1896; b) M. Scharrer, H. Noh, X. Wu, M. A. Anderson, A. Yamilov, H. Cao, R. P. H. Chang, *J. Opt.* **2010**, *12*, 024007; c) O. Toader, S. John, K. Busch, *Opt. Express* **2001**, *8*, 217; d) C.-F. Ying, W.-Y. Zhou, Q. Ye, X.-L. Zhang, J.-G. Tian, *J. Opt.* **2010**, *12*, 115101.

[12] a) C. Y. Cho, J. H. Moon, *Langmuir* **2012**, *28*, 9372; b) Y. G. Seo, M. A. Kim, H. Lee, W. Lee, *Sol. Energy Mater. Sol. Cells* **2011**, *95*, 332; c) J. H. Shin, J. H. Kang, W. M. Jin, J. H. Park, Y. S. Cho, J. H. Moon, *Langmuir* **2011**, *27*, 856.

[13] a) C. Dionigi, G. Calestani, T. Ferraroni, G. Ruani, L. F. Liotta, A. Migliori, P. Nozar, D. Palles, *J. Colloid Interface Sci.* **2005**, *290*, 201; b) J. W. Galusha, C.-K. Tsung, G. D. Stucky, M. H. Bartl, *Chem. Mater.* **2008**, *20*, 4925; c) F. Jia, W. Sun, J. Zhang, Y. Li, B. Yang, *J. Mater. Chem.* **2012**, *22*, 2435.

[14] a) B. Mandlmeier, N. K. Minar, J. M. Feckl, D. Fattakhova-Rohlfing, T. Bein, *J. Mater. Chem. A* **2014**, *2*, 6504; b) J. M. Szeifert, D. Fattakhova-Rohlfing, D. Georgiadou, V. Kalousek, J. Rathouský, D. Kuang, S. Wenger, S. M. Zakeeruddin, M. Grätzel, T. Bein, *Chem. Mater.* **2009**, *21*, 1260.

[15] V. G. Kessler, *J. Sol-Gel Sci. Technol.* **2013**, *68*, 464.

[16] a) J. J. De Yoreo, *MRS Bull.* **2017**, *42*, 525; b) L. B. Gower, *Chem. Rev.* **2008**, *108*, 4551; c) X. Ma, S. Zhang, F. Jiao, C. J. Newcomb, Y. Zhang, A. Prakash, Z. Liao, M. D. Baer, C. J. Mundy, J. Pfaendtner, A. Noy, C. L. Chen, J. J. De Yoreo, *Nat. Mater.* **2017**, *16*, 767; d) C. C. Perry, S. V. Patwardhan, O. Deschaume, *Biochem. Soc. Trans.* **2009**, *37*, 687.

[17] V. Thota, C. C. Perry, *Recent Pat. Nanotechnol.* **2017**, *11*, 168.

[18] A. Chemseddine, T. Moritz, *Eur. J. Inorg. Chem.* **1999**, *1999*, 235.

[19] L. Miao, P. Jin, K. Kaneko, A. Terai, N. Nabatova-Gabain, S. Tanemura, *Appl. Surf. Sci.* **2003**, *212*, 255.

[20] X. Xue, W. Ji, Z. Mao, H. Mao, Y. Wang, X. Wang, W. Ruan, B. Zhao, J. R. Lombardi, *J. Phys. Chem. C* **2012**, *116*, 8792.

[21] Y. Vasquez, M. Kolle, L. Mishchenko, B. D. Hatton, J. Aizenberg, *ACS Photonics* **2014**, *1*, 53.

[22] C. G. Granqvist, *Sol. Energy Mater. Sol. Cells* **2012**, *99*, 1.

[23] H. Li, G. Vienneau, M. Jones, B. Subramanian, J. Robichaud, Y. Djaoued, *J. Mater. Chem. C* **2014**, *2*, 7804.

[24] J. Goodwin, J. Hearn, C. Ho, R. H. Ottewill, *Colloid Polym. Sci.* **1974**, *252*, 464.